DOI: 10.1557/adv.2019.127



# Design and Simulation of the Bifacial III-V-Nanowire-on-Si Solar Cell

Anastasiia Fedorenko, Mohadeseh A. Baboli, Parsian K. Mohseni, and Seth M. Hubbard

Microsystems Engineering, NanoPower Research Laboratories, Rochester Institute of Technology, 156 Lomb Memorial Dr., Rochester, New York 14623, USA

ABSTRACT

Rigorous coupled wave analysis (RCWA) simulation was used to model the absorption in periodic arrays of  $GaAs_{0.73}P_{0.27}$  nanowires (NWs) on Si substrates dependent upon the diameter (D), length (L), and spacing (center-to-center distance, or pitch, P) of the NWs. Based on this study, two resonant arrangements for a top NW array sub-cell having the highest limiting short-circuit current densities ( $J_{sc}$ ) were found to be close to D=150 nm, P=250 nm and D=300 nm, P=500 nm, both featuring the same packing density of 0.28. Even though a configuration with thinner NWs exhibited the highest  $J_{sc}=19.46$  mA/cm², the array with D=350 nm and P=500 nm provided current matching with the underlying Si sub-cell with  $J_{sc}=18.59$  mA/cm². Addition of a rear-side  $In_{0.81}Ga_{0.19}As$  nanowire array with D=800 nm and P=1000 nm was found to be suitable for current matching with the front NW sub-cell and middle Si. However, with thinner and sparser  $In_{0.81}Ga_{0.19}As$  NWs with D=700 nm and P=1000 nm, the  $J_{sc}$  of the bottom sub-cell was increased from 17.35 mA/cm² to 18.76 mA/cm² using a planar metallic back surface reflector, thus achieving a current matching with the top and middle cells.

### INTRODUCTION:

Cost-competitive Si-based hybrid photovoltaic systems featuring high photoconversion efficiency can be realized through multijunction designs by combining Si and III-V materials [1, 2]. The manufacturing cost of III-V-on-Si solar cells can be further reduced by transitioning from thin-film to NW-based devices [3–5]. The radial spatial confinement of NWs allows for efficient strain relaxation, which enables direct epitaxy of a broad range of the lattice-mismatched materials on Si, thereby allowing unprecedented bandgap tunability and heterogeneous integration [5]. In addition, the rod-like shape of the NW can alter the photonic properties of the semiconductor material

https://doi.org/10.1557/adv.2019.127

making III-V NWs versatile for many optoelectronic device applications. By varying thickness and spatial distribution the NW optical response can be adjusted to provide either wavelength-selective sensing or broad-band absorptivity. In photovoltaics, the geometry-driven broad-band enhancement in light absorption promotes high short-circuit current density while the enforced directionality in the NW emission may cause the thermodynamic limit of open-circuit voltage to increase. These effects combined with efficient carrier extraction would allow the theoretical NW solar cell efficiency to potentially exceed the efficiency limit of thin-film planar devices [6, 7].

III-V-on-Si multijunction solar cells can be made using 1.75 eV GaAs<sub>0.73</sub>P<sub>0.27</sub> NWs on the front side of a bulk-type, planar Si solar cell and 0.5 eV In<sub>0.81</sub>Ga<sub>0.19</sub>As NWs on the rear side (the ideal bandgaps (Eg) are based on Shockley-Queisser detailed balance efficiency calculation for a fixed middle cell with  $E_g = 1.12$  eV). Absorption and limiting short-circuit current (J<sub>sc</sub>) in wide-bandgap GaAs<sub>0.73</sub>P<sub>0.27</sub> top-side NW arrays are highly geometry-sensitive. The J<sub>sc</sub> in an underlying Si cell also becomes a function of the diameter and pitch of the top array for a fixed NW length. Thus, an optimization of the dimensions of NWs relatively to their spatial distribution in array configurations is needed to achieving absorption enhancement promoting current matching between subcells. In this paper, a top-side NW array geometry that was optimized for maximum efficiency operation of a dual-junction solar cell as a part of a GaAs<sub>0.73</sub>P<sub>0.27</sub>/Si/ In<sub>0.81</sub>Ga<sub>0.19</sub>As triple-junction NW-based device (Fig. 1a) is reported. Additionally, adjustment of the rear-side 0.5 eV NW sub-cell was necessary, since unlike bulk materials, the diameter of the NWs affects the fundamental light scattering mechanism. For longer wavelengths, transmission of electromagnetic waves due to field screening can occur, thereby reducing the absorption in substantially thin In<sub>0.81</sub>Ga<sub>0.19</sub>As NWs compared to the planar films. At the same time, from the growth perspective, the use of thinner NWs would be preferable. Thus, modelling of the bottom array configurations focused on finding minimal NW diameters and reasonable pitch values that enable current matching between all three sub-cells.

### **SIMULATION DETAILS:**

The DiffractMOD simulation engine of Synopsys TCAD RSoft® software was used employing the RCWA technique for calculating absorption in GaAs<sub>0.73</sub>P<sub>0.27</sub> NW

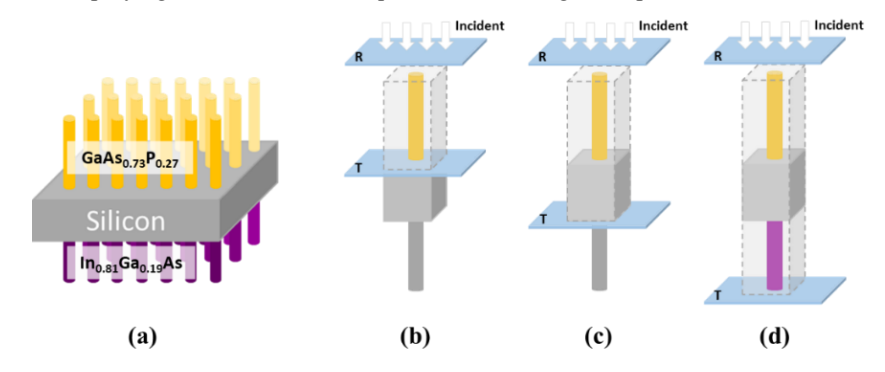


Figure 1. (a) Scheme of the bifacial 3J NW-on-Si solar cell (not to scale); Simulation domain with the reflection (R) and transmission (T) measurement planes for calculating absorption in (b) top NW array, (c) top array and Si middle cell, and (d) full 3J device.

arrays. A 3-dimensional unit cell with cubic arrangement of cylindrical NWs was created (Fig. 1b-d). A shallow underlying Si substrate was included in the simulation of the top NW array (Fig. 1b) to consider the possible impact of the NW/Si interface on the optical path of photons escaping the NW through transmission. Light absorption by NWs within the simulation domain was calculated as a difference between normalized incident, transmitted, and reflected components of linearly polarized normally incident light, which was enabled by the symmetry of the array making X- and Y-polarized waves indistinguishable, resulting in identical absorption spectra. The accuracy of the simulations was evaluated by increasing the number of the plane wave harmonics from 25 to 196 and examining the convergence of the diffraction efficiency spectra. This analysis was carried out for two diameters of the NWs, 150 nm and 350 nm. Using 10 harmonics per dimension (along X and Y where arrays are periodic), or a total of 100, results in convergence of the total integrated absorption within 0.2%. The error might be further minimized to 0.006% by transitioning to 13 harmonics per coordinate, however, in this case the computational speed would increase by a factor of 5, which was an important consideration for the batch simulations used in this work.

The diameters (D) of the NWs were varied in conjunction with the pitch (P), both with a step of 50 nm. The optimal length of the NWs mostly corresponds to the band edge absorption depth of GaAs<sub>0.73</sub>P<sub>0.27</sub>, so that an ideal length for the NWs alone would be several microns. However, the maximum efficiency of the multijunction solar cell requires not only maximization of J<sub>sc</sub>, but current matching between the sub-cells. Therefore, from the perspective of both experimental feasibility and current matching, L = 1.5 um was used.

To simulate the absorption in the middle Si cell with thickness of 200 μm, corresponding to a typical single-crystalline Si solar cell thickness, in relation to the pitch and diameter of the top NWs, the simulation unit cell was extended to comprise both the Si and top NW sub-cells (Fig. 1c). The total absorption in such stack was modelled for each geometry of the top array, and then the absorption in the middle cell was found by subtracting the initial top NWs absorption from the total absorption of the dual junction stack. The same approach was used to calculate the parameters of the bottom cell (Fig. 1d), except that the top array was included in the domain only in selected simulations where the pitches of the top and bottom NW arrays could be easily adjusted (for example,  $P_{Top} = 500$  nm,  $P_{Bot} = 1000$  nm). No anti-reflective coating, embedding polymer (for example benzocyclobutene, BCB, with refractive index of ~1.552), and ITO coatings were added to the simulated structure for the preliminary geometry optimization study in order to minimize the number of simulation parameters. For the current study, the thickness of the Si sub-cell was kept constant. The refractive indices and extinction coefficients of the ternary compounds used in simulations were calculated using the Kramers-Kronig model [8].

Limiting short-circuit current density, J<sub>sc,lim</sub>, calculations were performed based on the assumption that each absorbed photon generates an electron-hole pair and that 100% collection efficiency is realized, which can be described as generation current density, J<sub>Gen</sub>. Thus, J<sub>Gen</sub> values were calculated for the Air Mass 1.5 global (AM1.5G) incident spectrum with spectral irradiance  $I_{AMI.5G}(\lambda)$  taken from ASTM G173-03 Tables and solar cells absorption,  $A(\lambda)$  extracted from simulation as:

$$J_{sc,lim} \equiv J_{Gen} = \int_{\lambda_1}^{\lambda_2} \frac{q\lambda}{hc} I_{AM1.5G}(\lambda) A(\lambda) d\lambda. \tag{1}$$

In Eq. 1, the values of spectral irradiance of the AM1.5G spectrum were interpolated to match the wavelength step of the simulated absorption spectra (5 – 10 nm). This integral was then solved numerically for individual sub-cells with wavelengths from  $\lambda_1$  to  $\lambda_2$  corresponding to the absorption range of the sub-cell.

While simulations of absorption and calculation of the generation currents in the top array and middle Si cells were relatively straightforward, direct simulation of an entire 3J device, as shown on Fig. 1d, was associated with the necessity of matching the periodicities, or pitches, in top and bottom arrays within a single simulation domain. Thus, in order to map the J<sub>Gen</sub> of the bottom cell over a broad range of diameters and pitches, significantly more computational resources would be required. To facilitate the process and get a general guideline for the bottom NWs' parameters, an initial adjustment of the bottom In<sub>0.81</sub>Ga<sub>0.19</sub>As NW sub-cell's geometry was performed without a top-side array added on the Si surface to avoid the mismatch between the periodicity in top and bottom arrays. Using this approach, the diameters and pitches of the bottom NWs were swept from 300 nm to 1200 nm and from 350 nm to 1500 nm, respectively. However, since the front NW array acts as an antireflective coating, its impact on the absorption in the bottom array was evaluated by comparing the reflectivity spectra of the bare Si, R<sub>bare</sub>, and Si with the NW array on top, R<sub>ARC</sub>, in the absorption range of the bottom array (i.e. from ~1.2 μm to 2.5 μm). Thus, the maximum generation current that could be gained by the bottom NWs by including top array was calculated. For some cases where pitches of the top and bottom arrays are  $P_{\text{Top}} = 500 \text{ nm}$  and  $P_{\text{Bot}} = 1000 \text{ nm}$ , the whole structure was directly modelled by increasing the number of the top NWs inside the domain to form a  $2 \times 2$  array. The effects of a back-surface reflector (BSR) on the long-wavelength absorption in the solar cell were studied as well. In all cases, the BSR was represented by a flat Au slab in contact with the rear-side of the InGaAs NWs.

### RESULTS AND DISCUSSION:

Fig. 2a shows the maps of limiting  $J_{sc}$  extracted for the top NW array for the AM1.5G solar spectrum; Fig. 2b shows the difference between the  $J_{sc}$  values of the top

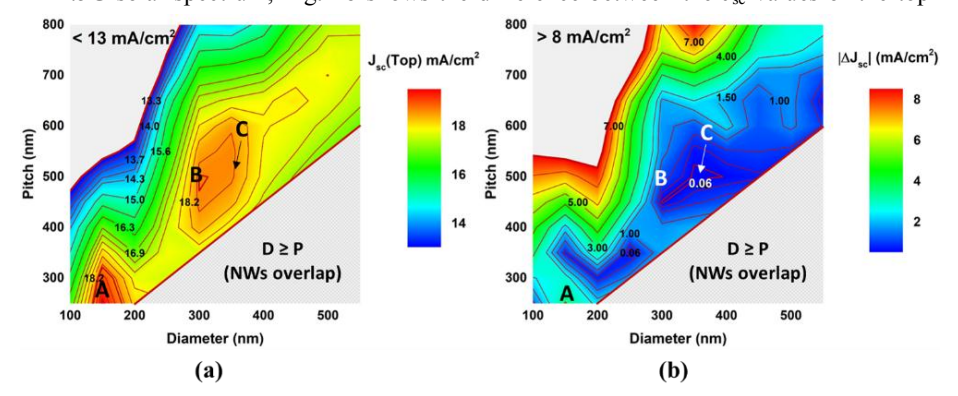


Figure 2. (a) Limiting short-circuit current density of the top GaAsP cell ( $J_{sc}(Top)$ ) mapped as a function of diameter and pitch of the NW array; (b) difference between  $J_{sc,lim}$  of the top GaAsP and middle Si cells ( $\Delta J_{sc}$ ). Arrays A, B, and C correspond to the dimensions  $D_A = 150$  nm and  $P_A = 250$  nm,  $D_B = 300$  nm and  $P_B = 500$  nm,  $D_C = 350$  nm and  $P_C = 500$  nm, respectively.

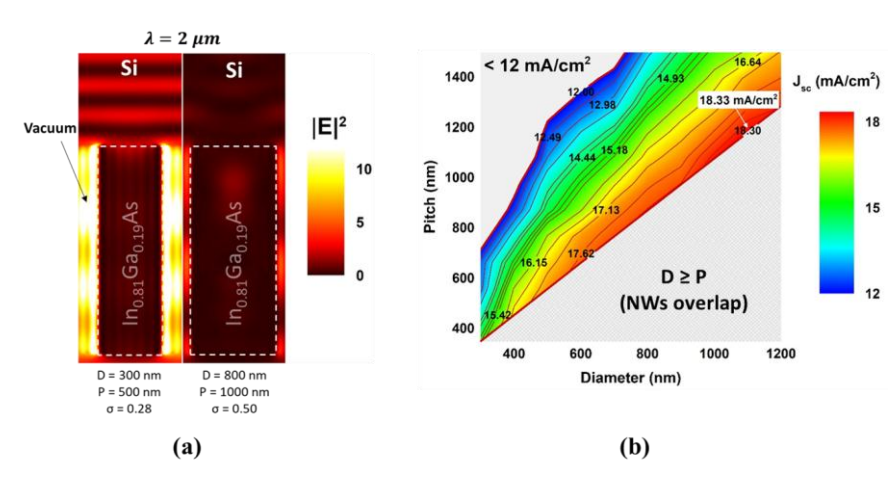


Figure 3. (a) Cross-sectional view of the electric field intensity in bottom InGaAs NW arrays on the rear side of 200  $\mu$ m-thick Si with D = 300 nm, P = 500 nm and D = 800 nm, P = 1000 nm in vacuum under monochromatic illumination with the wavelength of 2  $\mu$ m; (b) short-circuit current density of the bottom NW sub-cell as a function of NW diameter and pitch extracted from absorption simulations (without top NW array included); the cut-off region (< 12 mA/cm²) corresponds to the  $J_{sc}$  monotonously decreasing below 12 mA/cm².

GaAsP NW cell and middle Si cell in consideration that all absorbed flux is converted into electrical current. Absorption in the arrays where diameter of the NWs is equal or exceeds pitch was not simulated since it is not physical. The use of NWs not only provides higher photoconversion efficiency, but also allows for dramatic reduction in material volume (i.e., compared to lattice-mismatched thin film GaAsP-on-Si growth which may also include thick metamorphic buffers). Maximum current from both the top and middle cells can be provided with only 30 - 40% of the solid material otherwise required for planar devices. Converted to the mass of metalorganic precursors required for metalorganic vapour phase epitaxy (MOVPE) of NWs, this corresponds to an overall material savings of ~93% (not including the cost of several micrometres-thick metamorphic buffer in case of thin film). In Fig. 2a, two local  $J_{sc}$  maxima at  $D_A = 150$ nm,  $P_A = 250$  nm and  $D_B = 300$  nm,  $P_B = 500$  nm are observed for the AM1.5G spectrum. However, minimization of the difference between the current output from top and middle cell is critical for approaching the maximum possible efficiency of the full triple-junction cell, assuming that the bottom cell with its 0.5 eV bandgap is not current-limiting. Although arrangement A ( $D_A = 150$  nm and  $P_A = 250$  nm) would allow realization of a maximum  $J_{sc}(AM1.5G) = 19.65 \text{ mA/cm}^2$ , this configuration would not be preferable for a tandem-junction solar cell design, as it would make the middle cell current-limiting with 3.05 mA/cm<sup>2</sup> overproduction from the top cell. In this regard, the use of configuration B  $(D_B = 300 \text{ nm} \text{ and } P_B = 500 \text{ nm})$  can be more beneficial. However, as seen in Fig. 2b, an alternative array configuration C with  $D_C = 350$  nm and  $P_C = 500$  nm will provide current matching between top and middle cells with  $|\Delta J_{sc}| = 0.01$  mA/cm<sup>2</sup>. The packing density  $(\sigma)$ , which is defined as the ratio of NW cross-sectional area to unit cell area (i.e., equal to pitch squared), is slightly higher for array C ( $\sigma_C = 0.39$ ) than for arrays A and B ( $\sigma_{A,B} =$ 0.28). While the difference between  $J_{sc}(A)$  and  $J_{sc}(B)$  does not exceed 1 mA/cm<sup>2</sup>, the difference in the J<sub>sc</sub> offsets between top and middle cells is drastic (Fig. 2b). Interestingly, the packing density of NWs in both A and B configurations remains equal, which implies

that scattering at the NW/vacuum interface may be responsible for attenuation in the Si sub-cell absorption.

In practice, the proposed top cell design C providing  $J_{sc}(C) = 18.59 \text{ mA/cm}^2 \text{ can}$ be realized via selective-area growth (SAG) by MOVPE using electron beam lithography (EBL) or nanoimprint lithography for pre-growth periodic pattern generation [9]. For the bottom cell growth following the SAG of the top GaAs<sub>0.73</sub>P<sub>0.27</sub> NWs array, it would be preferable to avoid any added pre-growth patterning steps. Therefore, template-free selfassembly of In<sub>0.81</sub>Ga<sub>0.19</sub>As NWs on Si is suggested as the growth method [10]. By tuning the growth parameters, the self-assembly method tends to yield higher number density arrays of thin NWs, or larger-diameter NWs with sparse arrangement [11]. However, for the NWs with D  $\ll \lambda$ , electric field screening induced by a high refractive index contrast between the NWs and surrounding medium (e.g., vacuum, BCB, etc.) and strong reflection of IR light at the Si-NW interface occurs, leading to reduced absorption and current generation from the bottom array. Figure 3a illustrates these effects by comparing intensities of the electric field in the cross-section of the InGaAs NWs (with D = 300 nm, P = 500 nm and D = 800 nm, P = 1000 nm) and surrounding medium (here, vacuum) on the rear side of Si slab under monochromatic illumination with wavelength of 2 µm at which absorption in thin NWs is considerably low compared to that of thicker NWs. Thus, in the triple-junction device, the bottom cell can become current-limiting, so that an increase in the single bottom NW's optical cross-section for IR light operation becomes necessary [12].

To further evaluate this point, the dependency of J<sub>sc</sub> of the back-side InGaAs sub-cell upon the NW diameter and pitch was studied. Here, the assumed ordering of NWs within the back-side array grown by template-free self-assembly is an approximation that can provide an evaluation of the influence of the physical NW crosssection and array packing density on the absorption cross-section. Considering the weak resonant behaviour of the bottom NW array in the IR range, these results can still be applicable to the self-assembled NW arrays with no long-range ordering, however, this point needs to be studied in more detail. Due to the significant mismatch between the size of the bottom array unit cell and unit cell of the top array, the simulation of the In<sub>0.81</sub>Ga<sub>0.19</sub>As NWs absorption as a function of D and P was performed without inclusion of the top array. J<sub>sc</sub>(Bottom) values calculated from such absorption simulations are plotted on Fig. 3b. Maximum  $J_{sc} = 18.33 \text{ mA/cm}^2$  was found at NW D = 1.1  $\mu$ m and P = 1.2 µm. Since GaAsP NWs on the front surface of Si exhibit anti-reflective properties, the true expected J<sub>sc</sub> value attributed to the back-side InGaAs sub-cell can be up to 5 mA/cm<sup>2</sup> higher than that mapped in Fig. 3b (from comparison of bare Si vs. Si with top NW array reflectivity spectra beyond 1.2 µm as discussed in the prior section), dependent on the diameter of rear-surface NWs and the dominant absorption loss mechanism. Thus, rearsurface NWs with D  $\leq$  1.1  $\mu$ m may also be considered.

To directly calculate the gain in current enabled by adding the top array C, absorption in the bottom array of  $In_{0.81}Ga_{0.19}As$  NWs with D = 800 nm and P = 1.0  $\mu$ m was simulated with the top  $2 \times 2$  array with configuration C introduced into the simulation domain as depicted on Fig. 1d. Reduction in front-surface reflection due to added top NW array promoted an increase in the bottom cell generation current by 2.95 mA/cm<sup>2</sup> resulting in total  $J_{sc} = 20.35$  mA/cm<sup>2</sup>. Since this value significantly exceeds the target limiting J<sub>sc</sub>'s of the top and bottom cells, an arrangement of thinner NWs was simulated with the top array as well. Taking into account the trade-off between the NW number density and NW thickness enforced by the growth mechanism [11], a reduction in NW diameters along with an increase in pitch would be preferred. To enable smaller

https://doi.org/10.1557/adv.2019.127

NW diameters whilst preserving the pitch of 1  $\mu$ m, a back surface reflector (BSR) layer was placed on the rear side of the planarized array. The BSR mitigated transmission loss through the array and allowed to increase the optical path length of long-wavelength photons by increasing the number of passes of light through the array. Thus, for an InGaAs NW array with D = 700 nm and P = 1  $\mu$ m with initial  $J_{sc}$  = 17.35 mA/cm² (simulated with top NWs in configuration C), adding a BSR results in an additional 1.41 mA/cm² of current density. The introduction of a BSR, therefore, generates a current-matched condition to the upper sub-cells ( $J_{sc}$ (Top) = 18.59 mA/cm²,  $J_{sc}$ (Middle) = 18.58 mA/cm², and  $J_{sc}$ (Bottom + BSR) = 18.76 mA/cm²) without physically pushing the length of the NWs to several microns. The key problem, however, is reflection at the interface between Si and thin  $In_{0.81}Ga_{0.19}As$  NWs at normal incidence of light. This can likely be addressed by adjusting the refractive index of the encapsulation medium, since anisotropic effective medium approximation fails for highly directionally aligned NWs and reflection at the interface is not purely a function of the volumetric fraction of the NWs [13].

### **CONCLUSIONS:**

Nanowire configurations in the top-side sub-cell of a triple-junction GaAs<sub>0.73</sub>P<sub>0.27</sub>/Si/In<sub>0.81</sub>Ga<sub>0.19</sub>As solar cell were optimized for achieving maximum J<sub>sc</sub> matched to the underlying Si sub-cell under AM1.5G illumination with the length of NWs fixed at 1.5 µm. Geometry-based J<sub>sc</sub> enhancement in the top sub-cell for  $GaAs_{0.73}P_{0.27}$  NW diameters in the 100 nm to 550 nm range is most pronounced at D = 150 nm and P = 250 nm, although an optimal arrangement providing current matching with Si is realized for D = 350 nm and P = 500 nm at  $J_{sc}$  = 18.59 mA/cm<sup>2</sup>. A rear-side 0.5 eV sub-cell composed of an array of In<sub>0.81</sub>Ga<sub>0.19</sub>As NWs operating in the wavelength region below the Si bandgap exhibited a significant loss in light coupling for NWs with diameters below ~400 nm, which likely results from both strong reflection at Si/NW interface and screening of the electric field by the adjacent NWs. By taking into account the impact of the top-side array on reflection in the IR range and adding a flat Au BSR, the minimum diameter of rear-side array NWs can be brought to D = 700 nm with P = 1μm. Further studies related to the optimization of the rear-surface sub-cell, including an encapsulation medium engineering and various approaches to BSR formation to increase absorption in the long wavelength range, are in progress as well as the study of electrical performance of the triple-junction device.

## **ACKNOWLEDGMENTS:**

This material is based upon work supported by the National Science Foundation under Award No. 1665086.

#### **References:**

[1] R. Cariou et al., "III-V-on-silicon solar cells reaching 33% photoconversion efficiency in two-

- terminal configuration," Nat. Energy, vol. 3, no. 4, pp. 326-333, 2018.
- [2] B. Bläsi et al., "Photonic structures for III-V/Si multijunction solar cells with efficiency >33%," Photonics Sol. Energy Syst. VII, vol. 10688, no. June, pp. 1068803-1-106883-11, 2018.
- [3] M. T. Borgström et al., "Towards Nanowire Tandem Junction Solar Cells on Silicon," *IEEE J. Photovoltaics*, vol. 8, no. 3, pp. 733–740, 2018.
- [4] S. Lourdudoss et al., "Trends in heteroepitaxy of III-Vs on silicon for photonic and photovoltaic applications," in *Smart Photonic and Optoelectronic Integrated Circuits XIX*, 2017, vol. 10107, no. February 2017, p. 1010705.
- [5] G. Kästner and U. Gösele, "Stress and dislocations at cross-sectional heterojunctions in a cylindrical nanowire," *Philos. Mag.*, vol. 84, no. 35, pp. 3803–3824, 2004.
- [6] N. Anttu, "Shockley-queisser detailed balance efficiency limit for nanowire solar cells," ACS Photonics, vol. 2, no. 3, pp. 446–453, 2015.
- [7] J. E. M. Haverkort, E. C. Garnett, and E. P. A. M. Bakkers, "Fundamentals of the nanowire solar cell: Optimization of the open circuit voltage," *Appl. Phys. Rev.*, vol. 5, no. 3, p. 031106, 2018.
- [8] S. Adachi, "Refractive indices of III-V compounds: Key properties of InGaAsP relevant to device design," J. Appl. Phys., vol. 53, no. 8, pp. 5863–5869, 1982.
- [9] B. A. Wood, P. Kuyanov, M. Aagesen, and R. R. LaPierre, "GaAsP nanowire-on-Si tandem solar cell," *J. Photonics Energy*, vol. 7, no. 04, p. 1, 2017.
- [10] G. Koblmüller and G. Abstreiter, "Growth and properties of InGaAs nanowires on silicon.," Phys. state solidi - Rapid Res. Lett., vol. 8, no. 1, pp. 11–30, 2013.
- [11] M. A. Baboli *et al.*, "Improving pseudo-van der Waals epitaxy of self-assembled InAs nanowires on graphene via MOCVD parameter space mapping," *CrystEngComm*, no. DOI:10.1039/C8CE01666F, p. DOI:10.1039/C8CE01666F, 2019.
- [12] J. Svensson, N. Anttu, N. Vainorius, B. M. Borg, and L. E. Wernersson, "Diameter-dependent photocurrent in InAsSb nanowire infrared photodetectors," *Nano Lett.*, vol. 13, no. 4, pp. 1380– 1385, 2013
- [13] H. Wang, X. Liu, L. Wang, and Z. Zhang, "Anisotropic optical properties of silicon nanowire arrays based on the effective medium approximation," *Int. J. Therm. Sci.*, vol. 65, pp. 62–69, 2013.